American Journal of Pharmacological Sciences, 2026, Vol. 14, No. 1, 7-19
Available online at http://pubs.sciepub.com/ajps/14/1/2
Published by Science and Education Publishing
DOI:10.12691/ajps-14-1-2

Docking-Based Evaluation of Defensin-Derived Peptides and Their Cu^{2+} Complexes as Dual-Target Inhibitors of Exo-β-(1,3)-Glucanase and Penicillin-Binding Protein Transglycosidase 1B

Olatomide A. Fadare[1,*], Temitayo O. Aiyelabola[1], Imisioluwa A. Akintola[2], Janet I. Michael[1], Rachael Y. Fadare[1], Chiamaka V. Chukwu[1], Folakemi O. Yakubu[1], Deborah A. Sanni[1], Roheemah O. Lawal[1], Akitsu Takashiro[3,*], Adenike Kuku[2]

[1]Department of Chemistry, Obafemi Awolowo University, Ile-Ife, Nigeria
[2]Department of Chemical Sciences, Kings University, Ode Omu, Osun State, Nigeria
[3]Department of Chemistry, Faculty of Science, Tokyo University of Science, Japan
*Corresponding author: tofadare@oauife.edu.ng, akitsu2@rs.tus.ac.jp

Received March 27, 2026; Revised April 29, 2026; Accepted May 05, 2026

Abstract The escalating crisis of antimicrobial resistance necessitates the discovery of novel therapeutic agents with distinct mechanisms of action. Herein, we report a molecular docking study evaluating fourteen short amphiphilic peptides (FLK1–FLK14), designed by harvesting positively charged clusters from defensins identified in Nigerian edible plants and their corresponding Cu^{2+} complexes against two essential microbial enzymes: *Candida albicans* exo-β-(1,3)-glucanase (antifungal target) and *Escherichia coli* penicillin-binding protein 1B transglycosylase (antibacterial target). All uncomplexed peptides exhibited superior binding affinities relative to the native glucanase inhibitor (NFG, −5.4 kcal/mol), with values ranging from −6.0 to −7.7 kcal/mol against glucanase and −5.5 to −7.0 kcal/mol against PBP1B. Cu^{2+} complexation produced diametrically opposed effects on the two targets: dramatic enhancement of glucanase binding (with affinities reaching −14.81 kcal/mol for FLK11–Cu^{2+} derived from pawpaw defensin) versus near-universal loss of binding to PBP1B. Interaction fingerprint analysis revealed that Cu^{2+} complexation promotes an "interaction saturation" state within the glucanase catalytic pocket, increasing hydrogen bonding (from 3–4 to 5–6) and electrostatic contacts (from 1–2 to 3–4), consistent with metal-induced preorganization of peptide surface chemistry. In contrast, the rigid, quasi-spherical Cu^{2+}–peptide assemblies were sterically incompatible with the narrow hydrophobic groove of PBP1B, leading to impaired active-site penetration despite preserved surface charge. Lead candidates identified for experimental validation include FLK11–Cu^{2+} (*pawpaw defensin*) and FLK12–Cu^{2+} (*tomato defensin*) for antifungal development, and uncomplexed FLK1 (*avocado*), FLK5 (*pawpaw*), FLK11 (*pawpaw*), FLK13 (*tomato*), and FLK14 (*tomato*) for antibacterial applications. Collectively, these findings establish a structure–activity framework for the rational design of pathogen-selective metallopeptide inhibitors derived from locally available plant sources and demonstrate that metal coordination can function as a switchable modality to tune target selectivity rather than a universally beneficial modification.

Keywords: *peptides, exo-β-(1,3)-glucanase, penicillin-binding protein 1B, antimicrobial resistance, molecular docking, metallopeptides*

Cite This Article: Olatomide A. Fadare, Temitayo O. Aiyelabola, Imisioluwa A. Akintola, Janet I. Michael, Rachael Y. Fadare, Chiamaka V. Chukwu, Folakemi O. Yakubu, Deborah A. Sanni, Roheemah O. Lawal, Akitsu Takashiro, and Adenike Kuku, "Docking-Based Evaluation of Defensin-Derived Peptides and Their Cu^{2+} Complexes as Dual-Target Inhibitors of Exo-β-(1,3)-Glucanase and Penicillin-Binding Protein Transglycosidase 1B." *American Journal of Pharmacological Sciences*, vol. 14, no. 1 (2026): 7-19. doi: 10.12691/ajps-14-1-2.

1. Introduction

The escalating crisis of antimicrobial resistance (AMR) has rendered many conventional antibiotics ineffective, creating an urgent global health imperative to discover novel therapeutic agents with distinct mechanisms of action [1]. Among the most promising alternatives are antimicrobial peptides (AMPs), which are evolutionarily conserved components of the innate immune system exhibiting broad-spectrum activity against bacteria, viruses, and fungi [2]. Defensins, are a major class of AMPs, are cationic host-defense peptides characterized by their conserved cysteine-stabilized architecture and multifaceted antimicrobial mechanisms, including membrane disruption, immunomodulation, and metabolic interference [3]. These properties position defensin-

derived peptides as attractive scaffolds for therapeutic development against multidrug-resistant pathogens [4].

A defining structural feature of defensins is the presence of clusters of positively charged amino acids (lysine, arginine, histidine) that create regions of net positive charge on their molecular surface [5]. These cationic clusters (Figure 1) facilitate electrostatic attraction to negatively charged lipid membranes and protein moieties on microbial cell surfaces, representing the initial and essential step in antimicrobial activity [6]. This charge-mediated targeting underlies the selectivity of defensins for microbial cells over mammalian cells, as bacterial and fungal membranes possess significantly higher negative charge densities due to their abundance of anionic phospholipids and teichoic acids [7].

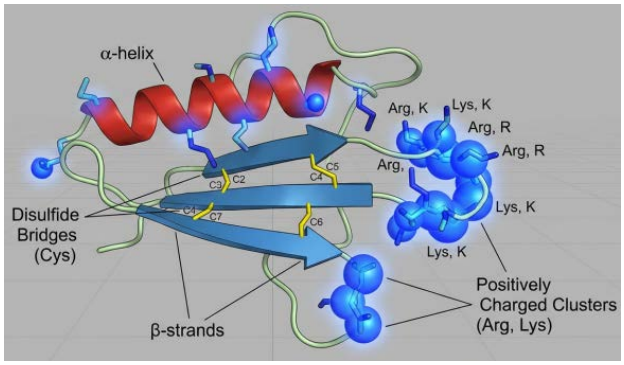

Figure 1. 3D diagram of a typical defensin with the clusters of positively charged amino acids highlighted, also showing the role that the cystein plays in tying up the defensin in a ribbonlike structure

Natural biodiversity offers a rich reservoir of defensin peptides with potential therapeutic applications. Notably, edible plants native to various regions, including Nigeria, represent an under-explored source of bioactive defensins with established safety profiles due to their long history of human consumption [8]. Recent studies have identified and characterized defensins from several locally consumed plant species. The J1-1 defensin from chilli pepper (*Capsicum annuum*) exhibits potent antifungal activity mediated by its cysteine-stabilized structure [9]. PaDef, isolated from avocado (*Persea americana*), demonstrates broad-spectrum antimicrobial properties and contains multiple cationic clusters essential for membrane interaction [10]. The tomato (*Solanum lycopersicum*) defensin, tdAmp1, has been characterized for its role in plant defense and presents unique sequence motifs with therapeutic potential [11]. Pawpaw (*Carica papaya*) expresses Pdf1.1, a defensin with characteristic cysteine-stabilized architecture that has yielded multiple bioactive peptide fragments [12], while maize (*Zea mays*) ZMDEF1 [13] contributes to the growing repertoire of plant-derived antimicrobial peptides. These naturally occurring defensins from locally consumed plants provide validated templates for peptide design, offering the advantage of inherent biocompatibility and reduced toxicity concerns.

Despite the promise of full-length defensins, their therapeutic development faces significant challenges. The large molecular size (typically 30–50 amino acids), complex three-dimensional structures stabilized by multiple disulfide bonds, and consequent difficulty of chemical synthesis pose substantial obstacles to manufacturing and clinical translation [14]. Furthermore, the structural complexity of native defensins can limit tissue penetration and increase susceptibility to proteolytic degradation [15]. These limitations have motivated interest in developing shorter peptide derivatives that retain the essential antimicrobial features of their parent molecules while offering improved synthetic accessibility and pharmacological properties [16].

The strategic approach of harvesting positively charged amino acid clusters from known defensins to generate short, amphiphilic peptides represents a rational design strategy with multiple advantages. By excising the cationic clusters responsible for membrane targeting and combining them with adjacent hydrophobic residues that facilitate membrane insertion, it is possible to create peptides that preserve the amphipathic character essential for antimicrobial activity [17]. Such short peptides (typically 5–15 amino acids) can be readily synthesized using solid-phase peptide synthesis, enabling cost-effective production and facile sequence optimization [18]. If these defensin-derived short peptides exhibit antimicrobial activity comparable to their full-length progenitors, this would represent a significant step forward in developing new, synthetically accessible antimicrobial agents [19].

An emerging strategy to further enhance antimicrobial peptide efficacy involves complexation with divalent metal ions, particularly Cu^{2+} and Zn^{2+} [20]. Metal coordination can profoundly influence peptide structure, stability, and biological activity through multiple mechanisms: (i) inducing specific bioactive conformations, (ii) facilitating membrane interactions, (iii) enabling metal-mediated oxidative damage to microbial targets, and (iv) modulating immunomodulatory properties [21]. The precise effects depend critically on peptide sequence, metal ion identity, coordination geometry, and ligand field characteristics, with the amino acid composition of the peptide—particularly the presence of histidine, cysteine, and methionine residues—determining metal-binding capacity and coordination mode [22]. Copper(II) complexes, in particular, have demonstrated enhanced antimicrobial activity against both bacterial and fungal pathogens [23], yet the structural basis for this potentiation at the level of specific enzyme–inhibitor interactions remains incompletely characterized.

Fungal pathogens pose a particular challenge due to the structural complexity of their cell walls, which serve as both a protective barrier and a dynamic interface for host interactions. The fungal cell wall is primarily composed of β-1,3-glucan polymers cross-linked with chitin, and its remodeling during growth and infection involves an array of glycosyl hydrolases [24]. Exo-β-(1,3)-glucanases, belonging to glycosyl hydrolase family 5, catalyze the processive release of glucose residues from the non-reducing ends of β-1,3-glucan chains, contributing to cell wall integrity, morphogenesis, and virulence [25]. The crystal structure of the *Candida albicans* exo-β-(1,3)-glucanase (Exg) reveals a distorted $(\beta/\alpha)_8$ barrel architecture with a deep catalytic pocket formed by extended loop regions, wherein two conserved glutamate residues (Glu192 and Glu296) function as nucleophile and acid/base catalysts, respectively, with Glu27 serving a dominant hydrogen-bonding role in substrate recognition [25]. Beyond its role in fungal physiology, this enzyme

generates β-1,3-glucan fragments that can be recognized as pathogen-associated molecular patterns (PAMPs) by host immune systems; consequently, fungal pathogens have evolved strategies to suppress this immune recognition, underscoring the enzyme's centrality in host–pathogen dynamics [4].

In parallel, bacterial cell wall synthesis represents one of the most successful targets for antibiotic intervention. Penicillin-binding proteins (PBPs) are membrane-anchored enzymes that catalyze the final stages of peptidoglycan biosynthesis, specifically the transglycosylation (glycan chain elongation) and transpeptidation (cross-linking) reactions [26]. Class A PBPs, such as PBP1B, are bifunctional enzymes containing both transglycosylase (TG) and transpeptidase (TP) domains. While β-lactam antibiotics have historically targeted the transpeptidation step, the transglycosylase domain remains underexploited therapeutically [27]. Moenomycin, a natural product complex, is the only known potent inhibitor of bacterial transglycosylases, exhibiting nanomolar affinity through interactions that require the full-length enzyme including its transmembrane domain [28]. However, moenomycin's poor pharmacokinetic properties have restricted its clinical use to animal growth promotion, highlighting the need for novel TG inhibitors [26]. The crystal structure of PBP1B in complex with moenomycin reveals a hydrophobic groove essential for substrate binding and enzymatic activity, with the transmembrane domain playing a critical role in membrane anchoring and substrate recognition [26].

Computational approaches have revolutionized the discovery and optimization of bioactive peptides [29]. Molecular docking, in particular, enables high-throughput screening of peptide libraries against target proteins by predicting binding modes and estimating binding affinities, thereby accelerating the identification of lead candidates while reducing time and cost relative to purely experimental approaches [30]. Recent advances in docking algorithms, integration with artificial intelligence, and enhanced molecular dynamics sampling have substantially improved the reliability of peptide–protein interaction predictions [31]. When combined with detailed interaction analysis—including hydrogen bonding networks, electrostatic complementarity, and hydrophobic contacts—docking studies provide mechanistic insights that guide rational peptide design and optimization [32]. However, comprehensive evaluations of docking programs for peptide–protein systems have revealed that while sampling power is generally adequate, scoring functions display limited performance in predicting absolute binding affinities, underscoring the importance of experimental validation [31].

In the present study, we designed a library of fourteen short amphiphilic peptides (designated FLK1–FLK14) by extracting positively charged amino acid clusters from defensins identified in Nigerian edible plants, including chilli pepper, avocado, tomato, pawpaw, maize, and broad bean. These peptides were engineered to retain the cationic character essential for microbial targeting while incorporating adjacent hydrophobic residues to preserve amphipathicity. We employed molecular docking to evaluate the binding affinities and interaction profiles of these peptides and their corresponding Cu^{2+} complexes against two essential microbial enzymes: *Candida albicans* exo-β-(1,3)-glucanase (a fungal cell wall remodeling enzyme) and *Escherichia coli* penicillin-binding protein 1B transglycosidase (a bacterial cell wall synthesis enzyme). We benchmark our findings against the native glucanase inhibitor (NFG) and the established antibacterial agents moenomycin and acyl-cephalexin. Through detailed analysis of hydrogen bonding, electrostatic interactions, hydrophobic contacts, and catalytic site engagement, we elucidate how peptide sequence diversity influences binding behavior and how metal coordination differentially modulates interactions with structurally distinct targets. Our findings identify high-priority lead candidates for experimental validation and establish a structure-activity framework for the rational design of pathogen-selective peptide inhibitors derived from naturally occurring defensins.

2. Methodology

2.1. Protein Target Preparation

The three-dimensional structures of the two target proteins were obtained from the RCSB Protein Data Bank (PDB). The crystal structure of exo-β-(1,3)-glucanase from *Candida albicans* was retrieved, 2PB1, while the structure of penicillin-binding protein 1B (1MWT) transglycosidase domain from *Escherichia coli* was retrieved from the protein data bank. Both structures were selected based on their resolution, completeness, and relevance to the microbial targets under investigation.

Prior to docking simulations, protein structures were prepared using AutoDock Tools (ADT, version 1.5.7) [33]. The preparation protocol involved: (i) removal of crystallographic water molecules and heteroatoms to prevent interference with docking calculations, (ii) addition of polar hydrogen atoms to enable accurate hydrogen bonding calculations, (iii) assignment of Gasteiger partial charges to all atoms, and (iv) merging of non-polar hydrogens to reduce computational complexity. The prepared proteins were subsequently saved in PDBQT format, which is compatible with AutoDock Vina and AutoDock 4.2 docking protocols [33,34].

2.2. Ligand Preparation

2.2.1. Defensin-Derived Peptide Design

A library of fourteen defensin-derived peptides (designated FLK1–FLK14) was designed by extracting positively charged amino acid clusters from the sequences of naturally occurring defensins identified in edible plants native to Nigeria. The source defensins and their corresponding peptide derivatives are presented in Table 1.

The design strategy focused on identifying contiguous sequence segments containing clusters of positively charged residues (arginine, lysine, histidine) with adjacent hydrophobic amino acids to preserve the amphipathic character essential for membrane interaction [34]. This approach yielded peptides ranging from 5 to 8 amino acids in length, with calculated net positive charges ranging from +1 to +5 at physiological pH. The final library

comprised fourteen unique sequences.

The three-dimensional structures of the peptides were generated using the Avogadro software, version 1.2, employing standard peptide bond geometry with energy minimization to relieve steric clashes. For docking simulations with AutoDock Vina, peptides were treated as flexible ligands with rotatable bonds assigned automatically by the software. Peptide structures were exported in PDB format and subsequently converted to PDBQT format using AutoDock Tools (ADT) [33].

Table 1. Source Defensins, Parent Sequences, Derived Peptides, and Literature References

Plant Source	Defensin Name	Full-Length Parent Sequence (Mature Domain)	Derived Peptide	Peptide Sequence	Net Charge	Source & Literature
Avocado (Persea americana)	PaDef	CETPSKHFNGLCIRSSNCASVC HGEHFTDGRCQGVRRRCMCLK PC	FLK1	TPSKHFN	+1	Guzmán-Rodríguez et al., 2013 (PaDef)
Avocado (Persea americana)	PaDef	CETPSKHFNGLCIRSSNCASVC HGEHFTDGRCQGVRRRCMCLK PC	FLK2	RRRCMCLK	+4	Guzmán-Rodríguez et al., 2013 (PaDef)
Maize (Zea mays)	ZMDEF1	RHCLSQSHRFKGLCMSSNNCA NVCQTENFPGGECKAEGATRK CFCKKIC	FLK3	QSHRFK	+2	Reported defensin (maize defensin family)
Maize (Zea mays)	ZMDEF1	RHCLSQSHRFKGLCMSSNNCA NVCQTENFPGGECKAEGATRK CFCKKIC	FLK4	TRKCFCKK	+4	Reported defensin (maize defensin family)
Pawpaw (Carica papaya)	Pdf1.1	QKLCERPSGTWSGVCGNSNAC KNQCINLEKARHGSCNYVFPAH KCICYFPC	FLK5	KARHGSC	+2	Pawpaw defensin identified (literature)
Pawpaw (Carica papaya)	Pdf1.1	QKLCERPSGTWSGVCGNSNAC KNQCINLEKARHGSCNYVFPAH KCICYFPC	FLK6	PAHKCIC	+1	Pawpaw defensin identified (literature)
Tomato (Solanum lycopersicum)	TPP3	Mature defensin domain of TPP3 (GenBank / PDB: 4UJ0)	FLK7	SCRKYC	+2	Baxter et al., 2015 (Tomato TPP3)
Tomato (Solanum lycopersicum)	TPP3	Mature defensin domain of TPP3 (GenBank / PDB: 4UJ0)	FLK8	HCSKLQ	+1	Baxter et al., 2015 (Tomato TPP3)
Tomato (Solanum lycopersicum)	TPP3	Mature defensin domain of TPP3 (GenBank / PDB: 4UJ0)	FLK9	RKCLCTK	+4	Baxter et al., 2015 (Tomato TPP3)
Chilli Pepper (Capsicum annuum)	J1-1	KICEALSGNFKGLCLKCSNKC	FLK10	KCSNKC	+2	Meyer et al., 1996 / Seo et al., 2014 (J1-1)
Pawpaw (Carica papaya)	Pdf1.1	QKLCERPSGTWSGVCGNSNAC KNQCINLEKARHGSCNYVFPAH KCICYFPC	FLK11	KARHGS	+2	Pawpaw defensin identified (literature)
Tomato (Solanum lycopersicum)	tdAmp1	MKIRASVRKICEKCRLIRRRGRI IVICSNPRHKQRQG	FLK12	SVRKIC	+2	Tomato plant defensin (bioinformatics/literature)
Tomato (Solanum lycopersicum)	tdAmp1	MKIRASVRKICEKCRLIRRRGRI IVICSNPRHKQRQG	FLK13	KCRLIRRR	+5	Tomato plant defensin (bioinformatics/literature)
Tomato (Solanum lycopersicum)	tdAmp1	MKIRASVRKICEKCRLIRRRGRI IVICSNPRHKQRQG	FLK14	RHKQRQ	+3	Tomato plant defensin (bioinformatics/literature)

2.2.2. Cu^{2+}–Peptide Complexes

Cu^{2+}–peptide complexes were constructed using a backbone-centric coordination model rather than enforcing residue-specific chelation at predefined side chains. This approach is supported by extensive coordination chemistry literature demonstrating that Cu^{2+} binding to short peptides is structurally plastic, often involving mixed N/O donor sets that include backbone amide nitrogens and carbonyl oxygens, with coordination modes varying with local environment and pH [13,22,35].

Each peptide was modeled to adopt a compact, globular conformation around the Cu^{2+} ion, in which peptide backbone amide carbonyl (C=O) and amide nitrogen (N–H) groups collectively contribute to metal coordination, forming a pseudo-spherical coordination environment (Figure 2). Such compact metallopeptide architectures are consistent with experimental and computational studies demonstrating multiple accessible coordination geometries and metal-induced folding in short peptides [21].

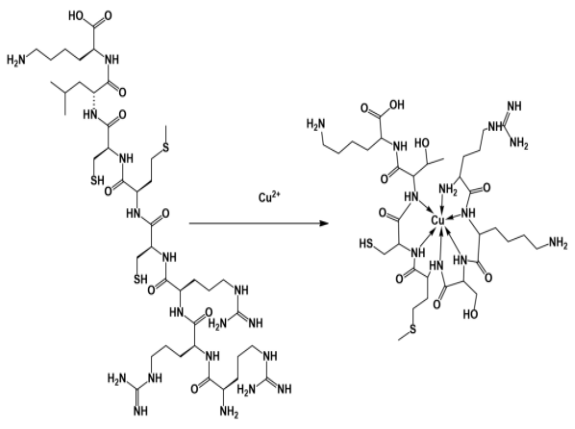

(a)

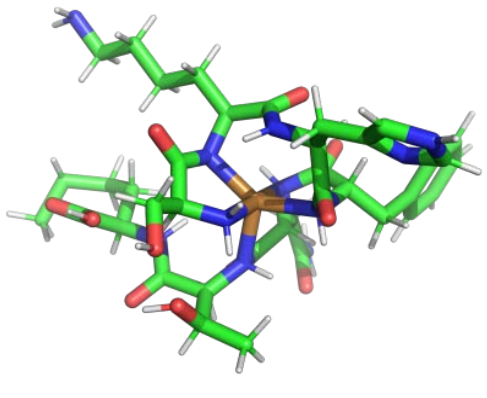

(b)

FLK2

Figure 2. (a) Diagramatic representation of peptide metal complex taking FLK2 as a sample and wraping the backbone around the Cu2+ to create the quasi spherical complex with amino acid residues pointing outwards

The Cu^{2+} ion was initially positioned near the geometric center of each peptide, followed by constrained local minimization to permit backbone wrapping around the metal center, producing compact Cu^{2+}–peptide assemblies suitable for docking. No explicit constraints were imposed to enforce side-chain chelation motifs; residues capable of metal interaction were permitted to contribute indirectly through proximal electrostatic and van der Waals interactions. This strategy reflects the experimentally observed polymorphism of Cu^{2+}–peptide coordination and avoids overfitting to any single chelation motif [13,22]. The resulting complexes were used for comparative docking and ranking of Cu^{2+}–complexed peptides.

Given that AutoDock Vina has inherent limitations in handling metal coordination bonds, the Cu^{2+}–peptide complexes were docked using AutoDock 4.2, which offers improved parameterization for metal ions [33]. The metal ion was treated as part of the ligand, with the entire complex defined as a single docking entity. Gasteiger charges were recalculated for the complete metal-peptide system, and atomic desolvation parameters were adjusted according to the AutoDock 4.2 force field specifications for metallocomplexes [36].

2.3. Molecular Docking Simulations

2.3.1. Docking of Uncomplexed Peptides (AutoDock Vina)

Molecular docking of the fourteen uncomplexed defensin-derived peptides against both target proteins was performed using AutoDock Vina, version 1.1.2, [34]. AutoDock Vina was selected for peptide-only docking due to its enhanced speed, improved scoring function, and superior accuracy in predicting binding modes of flexible ligands compared to its predecessor [37].

The docking grid boxes were defined to encompass the entire active site regions of each target protein. The grid box was centered around the catalytic site from which the native ligands were taken from, and the box size was set to cover the entire protein - ensuring coverage of the entire active site cleft and surrounding interaction surfaces. For each peptide–protein pair, docking simulations were performed with exhaustiveness set to 32 to enhance sampling of conformational space. The maximum number of binding modes generated was set to 20, with an energy range of 4 kcal/mol for output clustering. All other parameters were maintained at default values. The binding affinity (kcal/mol) for the top-ranked pose of each peptide was recorded, and poses were visually inspected to ensure reasonable orientation within the active site [34].

2.3.2. Docking of Cu^{2+}–Peptide Complexes (AutoDock 4.2)

Docking calculations for the Cu^{2+}–peptide complexes were conducted using AutoDock 4.2 [33], which provides specialized parameters for metallocomplex docking. The Lamarckian Genetic Algorithm (LGA) was employed for conformational searching and the grid boxes for AutoDock 4.2 simulations were defined identically to those used for AutoDock Vina to maintain consistency between the two docking protocols. Atomic affinity maps for all atom types present in the system, including the Cu^{2+} ion, were pre-calculated using AutoGrid 4.2. The Cu^{2+} ion was parameterized using the AutoDock 4.2 force field with appropriate solvation parameters and charge assignments (+2) [36]. Following completion of docking runs, the 10 generated conformations were clustered based on root-mean-square deviation (RMSD) with a tolerance of 2.0 Å. The lowest-energy conformation from the most populated cluster was selected as the representative binding mode for each Cu^{2+}–peptide complex [33].

2.4. Binding Affinity Analysis

For uncomplexed peptides, binding affinities were reported directly as AutoDock Vina scoring function outputs (kcal/mol), which approximate the Gibbs free energy of binding [34]. For Cu^{2+}–peptide complexes, AutoDock 4.2 estimated binding free energies were calculated using the force field-based scoring function, which includes terms for van der Waals interactions, hydrogen bonding, electrostatic interactions, desolvation, and torsional entropy [33].

To provide context for evaluating peptide performance, known inhibitors of each target were also docked as reference controls:

- For exo-β-(1,3)-glucanase: The native inhibitor (NFG) was docked using AutoDock Vina following the same protocol described for uncomplexed peptides.
- For PBP1B: Moenomycin and acyl-cephalexin were docked using AutoDock Vina, with grid boxes adjusted to accommodate their larger molecular sizes while maintaining coverage of the transglycosylase active site.

2.5. Visualization and Interaction Analysis

Post-docking analysis and visualization of protein–ligand interactions were performed using

PyMOL (version 2.5), Seeliger & de Groot, 2010, essentially for:

- Visual inspection of docked poses and validation of binding orientations
- Superimposition of peptide-bound structures with reference inhibitor-bound conformations
- Generation of publication-quality molecular graphics
- Measurement of interatomic distances between

peptide residues and protein active site atoms

For each top-ranked docking pose, the complete interaction fingerprint was recorded, including the specific amino acid residues involved in each interaction type. This analysis enabled correlation of binding affinity values with the underlying structural determinants of protein–ligand recognition.

2.6. Selection Criteria for Lead Candidates

Lead candidates for experimental validation were selected based on an integrated scoring system that considered:

1. Binding affinity (kcal/mol), with more negative values indicating stronger predicted binding
2. Number and quality of hydrogen bonds
3. Extent of electrostatic interactions and salt bridges
4. Degree of hydrophobic pocket occupation (classified as weak, moderate, or strong)
5. Confirmation of catalytic site engagement

For each target protein, the top-performing uncomplexed peptides and Cu^{2+} complexes were identified and prioritized for subsequent experimental validation.

3. Results and Discussion

3.1. Peptide Design and Rationale

The fourteen FLK peptides investigated in this study were derived from naturally occurring defensins identified in edible plant species commonly consumed in Nigeria, including chilli pepper, avocado, tomato, pawpaw, maize, and broad bean (Table 1). This design strategy offers several advantages: (i) the parent defensins have established antimicrobial activity and safety profiles due to their presence in consumed foods [9,10,11,12,13], (ii) the short peptides (5–8 amino acids) are amenable to cost-effective solid-phase synthesis [18], and (iii) retention of cationic clusters preserves the electrostatic targeting mechanism essential for microbial selectivity [6].

Methodological Considerations of Cu^{2+}–Peptide Modeling

The Cu^{2+}–peptide complexes in this study were constructed using a simplified backbone-centric coordination model rather than enforcing canonical side-chain chelation motifs typical of metalloproteins. This abstraction was adopted to avoid biasing docking outcomes toward predefined coordination geometries and to preserve conformational comparability across peptides of varying length and composition. While histidine- and cysteine-mediated chelation is common in native copper-binding proteins, enforcing such motifs a priori could obscure relative docking trends among short peptide fragments. Importantly, the uniform coordination paradigm enabled direct comparison of closely related peptides differing by single residues (e.g., FLK5 vs FLK11), facilitating evaluation of how side-chain composition influences predicted binding enhancement upon Cu^{2+} complexation. The resulting complexes should therefore be interpreted as comparative docking models rather than quantum-chemically optimized metallopeptide structures.

3.2. Differential Target Selectivity: Influence of Peptide Sequence on Binding

The defensin-derived peptide library demonstrated a striking dichotomy in its interaction profile with the two microbial targets, with binding affinities strongly influenced by peptide sequence characteristics. As shown in Table 2, all fourteen peptides exhibited favorable binding energies against exo-β-(1,3)-glucanase, ranging from -6.0 kcal/mol to -7.7 kcal/mol. In contrast, their affinity for Penicillin-Binding Protein Transglycosidase 1B (PBP1B) was generally lower, ranging from -5.5 to -7.0 kcal/mol (Table 3). This differential selectivity likely reflects the distinct physicochemical properties of each binding pocket. The glucanase presents a negatively charged catalytic pocket [25] that is electrostatically complementary to the cationic peptides, whereas the transglycosidase domain of PBP1B features a narrower hydrophobic groove [26] that is less accommodating to charged residues.

Sequence-specific effects were evident in the binding data. Against glucanase, the highest-affinity uncomplexed peptides were FLK7 (-7.7 kcal/mol), FLK2 (-7.4 kcal/mol), FLK4 (-7.5 kcal/mol), FLK8 (-7.4 kcal/mol), and FLK6 (-7.5 kcal/mol) (Figure 3). Notably, these top performers include peptides with both high net charge (FLK2, +4; FLK4, +4) and moderate charge (FLK7, +2; FLK8, +1; FLK6, +1), suggesting that factors beyond simple electrostatics—such as spatial arrangement of charged residues and hydrophobic character—contribute to binding optimization. The presence of cysteine residues in many top performers (FLK2, FLK4, FLK7, FLK8) may also influence binding through disulfide-mediated conformational stabilization [38].

Strikingly, every defensin-derived peptide exhibited superior binding affinity compared to the native glucanase inhibitor (NFG), which registered a binding score of -5.4 kcal/mol (Table 3), Figure 3 shows the binding mode of top 3 uncomplexed peptides. This baseline comparison validates the strategy of harvesting cationic clusters from natural defensins, demonstrating that short peptides retaining the essential charge features of their parent molecules can achieve potent enzyme inhibition [19].

For PBP1B, benchmarking against established antibacterial agents revealed that several uncomplexed peptides performed remarkably well. FLK1, FLK5, FLK13, and FLK14 exhibited binding affinities (ranging from -6.8 to -7.0 kcal/mol) highly comparable to acyl-cephalexin (-7.4 kcal/mol). Notably, FLK13—derived from tomato defensin tdAmp1 and possessing the highest net charge (+5)—achieved -6.8 kcal/mol, while FLK14 (also from tomato, +3) reached -6.9 kcal/mol. This suggests that the cationic clusters from tomato defensin are particularly well-suited for engaging the PBP1B active site, possibly due to optimal spacing of charged and hydrophobic residues [11].

Table 2. Docking Binding Affinities of Defensin-Derived Peptides and Cu^{2+} Complexes Against Exo-β-(1,3)-Glucanase & Penicillin-Binding Protein Transglycosidase 1B (PBP1B)

Ligand	Exo-β-(1,3)-Glucanase Peptide Binding Affinity (kcal/mol)	Exo-β-(1,3)-Glucanase Cu^{2+}–Peptide Complex Binding Affinity (kcal/mol)	PBP1B Peptide Binding Affinity (kcal/mol)	PBP1B Cu^{2+}–Peptide Complex Binding Affinity (kcal/mol)
FLK1	−6.7	−9.28	−6.9	−1.08
FLK2	−7.4	−8.55	−6.7	NIL
FLK3	−7.2	−10.55	−6.2	−2.01
FLK4	−7.5	−11.60	−5.7	−0.40
FLK5	−7.1	−11.48	−7.0	−1.81
FLK6	−7.5	−12.94	−5.5	−3.34
FLK7	−7.7	−12.52	−5.5	−4.11
FLK8	−7.4	−10.48	−6.3	−2.17
FLK9	−7.2	−9.87	−6.0	−1.42
FLK10	−6.0	−12.41	−5.9	−2.22
FLK11	−7.1	−14.81	−6.5	−3.99
FLK12	−7.0	−12.94	−6.1	−5.30
FLK13	−7.5	−6.71	−6.8	−1.87
FLK14	−7.1	−10.71	−6.9	−4.92
Native inhibitor (NFG)	−5.4	−5.4	—	—
Moenomycin	—	—	−9.1	—
Acyl-cephalexin	—	—	−7.4	—

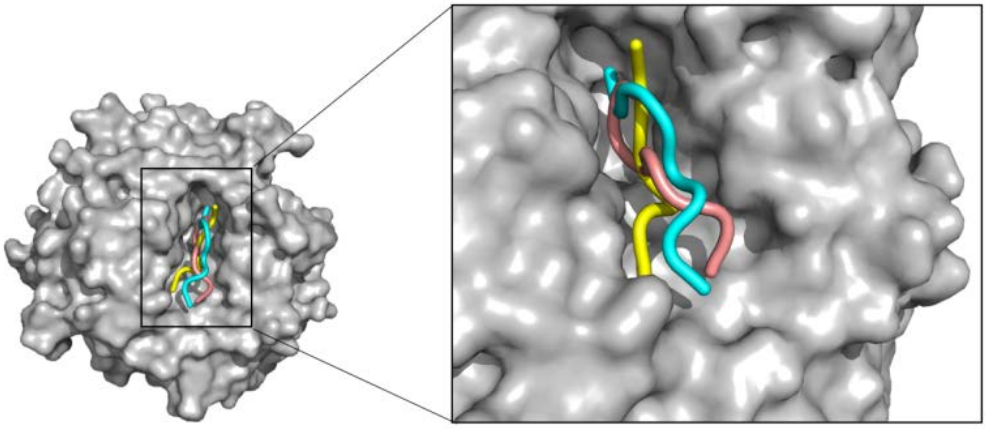

Figure 3. Binding modes of top-performing uncomplexed FLK peptides in the exo-β-(1,3)-glucanase active site. Representative docking poses of FLK4 (cyan), FLK6 (yellow), and FLK13 (brown) within the catalytic pocket of exo-β-(1,3)-glucanase. All three peptides occupy the substrate-binding groove and establish direct contacts with residues lining the catalytic site, illustrating how short, uncomplexed FLK peptides achieve comparable binding through distinct but convergent interaction patterns

3.3. Sequence-Dependent Effects of Cu^{2+} Complexation on PBP1B Binding

The docking results for PBP1B (Table 2) reveal a striking, sequence-dependent impact of Cu^{2+} complexation on peptide binding. In general, the Cu^{2+} complexes exhibit reduced affinity compared to their uncomplexed counterparts, reflecting the combined influence of steric hindrance and surface charge distribution. The backbone-centric coordination model positions the Cu^{2+} ion within a quasi-spherical peptide cage, with side chains oriented outward, resulting in increased rigidity of the overall ligand. This rigidity limits the ability of the Cu^{2+}–peptide complexes to penetrate the narrow hydrophobic pocket of PBP1B, particularly for peptides with larger or highly charged outer surfaces (Figure 4).

Most Cu^{2+} complexes show dramatic drops in binding affinity: FLK1 decreased from −6.9 kcal/mol to −1.08 kcal/mol, FLK5 from −7.0 kcal/mol to −1.81 kcal/mol, and FLK13 from −6.8 kcal/mol to −1.87 kcal/mol. FLK2–Cu^{2+} failed to produce a valid docking pose ("NIL"), suggesting steric incompatibility with the rigid pocket. These findings indicate that both the overall steric bulk introduced by metal complexation and the surface charge density of the peptide periphery are critical determinants of PBP1B recognition.

Interestingly, FLK12–Cu^{2+} (SVRKIC from tomato defensin tdAmp1) retained moderate binding (−5.30 kcal/mol). This peptide has a relatively balanced charge distribution on the outer surface of its Cu^{2+}-encapsulated sphere and a smaller hydrodynamic radius, allowing partial accommodation within the PBP1B groove. This observation highlights that even in the backbone-centric model, peptides with compact geometry and moderate

external cationicity can maintain interactions, despite the rigidity imposed by metal encapsulation. Collectively, these results demonstrate that Cu^{2+} complexation does not uniformly enhance binding; rather, the impact depends on peptide size, outer surface charge, and the steric constraints of the target pocket.

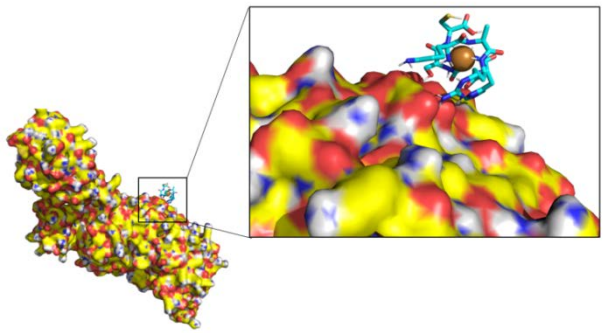

Figure 4. Representative binding pose of a Cu^{2+}–FLK complex at the surface of PBP1B, illustrating steric exclusion from the transglycosylase groove.The Cu^{2+}-complexed peptide (stick representation) fails to penetrate the narrow hydrophobic binding groove preferred by uncomplexed FLK peptides and instead remains superficially associated with the protein surface (electrostatic surface rendering: red, negative; blue, positive; white, neutral). Metal coordination increases steric bulk and alters charge distribution, preventing productive insertion into the catalytic cleft and resulting in a sparse interaction network relative to uncomplexed peptides. This provides a structural rationale for the catastrophic loss of PBP1B affinity observed upon Cu^{2+} complexation

3.4. Structural Basis for Glucanase Inhibition: Cu^{2+}-Mediated Interaction Saturation and Insights from Pawpaw Derivatives

In contrast to PBP1B, Cu^{2+} complexation markedly enhances binding to Exo-β-(1,3)-glucanase (Table 3), illustrating how sequence and structural context modulate metal-mediated activity. The overlapping fragments from pawpaw defensin (FLK5 and FLK11; and FLK6) provide particularly informative examples for understanding structure-activity relationships.

Uncomplexed peptides (FLK4, FLK6, FLK13) form 3–4 hydrogen bonds and 1–2 electrostatic contacts, with consistent engagement of the catalytic site (Figure 3). These data indicate that diverse sequences—varying in charge and hydrophobicity—can achieve similar baseline interactions with glucanase.

Cu^{2+}-mediated synergy is most pronounced for FLK11–Cu^{2+} (−14.81 kcal/mol), which exhibits 6 hydrogen bonds and 4 electrostatic interactions, nearly doubling the uncomplexed network. The Cu^{2+} ion acts as a central stabilizer within the peptide cage, facilitating optimal orientation of polar and charged side chains toward the active site. Notably, FLK5–Cu^{2+} (−11.48 kcal/mol) displays slightly lower enhancement, suggesting that the terminal cysteine in FLK5 may partially constrain backbone flexibility compared to FLK11, which lacks this residue. This subtle difference underscores how minor variations in sequence can profoundly influence metal-mediated interaction saturation. FLK12–Cu^{2+} (SVRKIC) also achieves high-affinity binding (−12.94 kcal/mol), demonstrating that multiple sequences, including those with fewer potential metal-coordinating residues, can attain strong glucanase inhibition through the backbone-encapsulated Cu^{2+} model.

These observations align with emerging evidence that metal coordination can amplify antimicrobial activity not solely by direct binding, but also via structural reorientation [20,23,39]. By combining steric stabilization with maximal exposure of functional side chains, Cu^{2+}–peptide complexes exploit both binding site complementarity and physicochemical enhancement (see Figure 5 & Figure 6), offering a dual mechanism for enzyme inhibition and antimicrobial efficacy.

3.5. Interaction Analysis of PBP1B Binding: Hydrophobic Dominance and Metal Steric Effects

Success of uncomplexed peptides: The top-performing uncomplexed ligands (Figure 7), particularly FLK5 (−7.0 kcal/mol, pawpaw defensin Pdf1.1) and FLK13 (−6.8 kcal/mol, tomato defensin tdAmp1), achieve high affinity by balancing hydrogen bonding with strong hydrophobic interactions (Table 4). FLK5 establishes 4 hydrogen bonds while achieving “Strong” occupation of the hydrophobic pocket, closely mimicking the gold-standard inhibitor moenomycin. Similarly, FLK13 forms 4 hydrogen bonds and 2 electrostatic interactions, comparable to acyl-cephalexin (Table 5). These data suggest that effective PBP1B inhibition requires flexible ligands capable of penetrating the narrow hydrophobic groove while maintaining optimal hydrogen-bonding networks [26].

Mechanistic explanation for Cu^{2+}-induced loss: Incorporation of the Cu^{2+} ion within the quasi-spherical peptide cage rigidifies the ligand and increases its steric footprint. In the narrow PBP1B binding groove, this structural bulk acts as a steric wedge, impeding deep penetration and preventing proper hydrophobic packing. Even when the side chains are oriented outward, the global rigidity reduces conformational adaptability, limiting the number of hydrogen bonds and electrostatic contacts achievable within the pocket. For example, FLK12–Cu^{2+} (−5.30 kcal/mol) can form only minimal interactions, which are insufficient to compensate for the loss of hydrophobic anchoring and optimal positioning.

Implications for ligand design: These results underscore that PBP1B inhibition is hydrophobically driven, requiring ligands that are sufficiently flexible and spatially compatible with the deep groove. Backbone-encapsulated metal complexes, while effective for enhancing interaction networks in other targets (e.g., glucanase), are detrimental for rigid, narrow protein pockets, highlighting the necessity of target-specific design strategies.

Table 3. Key Protein–Ligand Interactions for Top Peptides and Cu^{2+} Complexes Against Exo-β-(1,3)-Glucanase

Ligand	Binding Affinity (kcal/mol)	Hydrogen Bonds	Electrostatic / Salt Bridges	Hydrophobic Contacts	Catalytic Site Engagement
FLK4	−7.5	3	2	Moderate	Yes
FLK6	−7.5	4	2	Moderate	Yes
FLK13	−7.5	3	1	Moderate	Yes
FLK5–Cu^{2+}	−11.48	5	3	Strong	Yes
FLK11–Cu^{2+}	−14.81	6	4	Strong	Yes
FLK6–Cu^{2+}	−12.94	5	3	Strong	Yes
FLK12–Cu^{2+}	−12.94	5	3	Strong	Yes
NFG (inhibitor)	−5.4	2	1	Weak	Yes

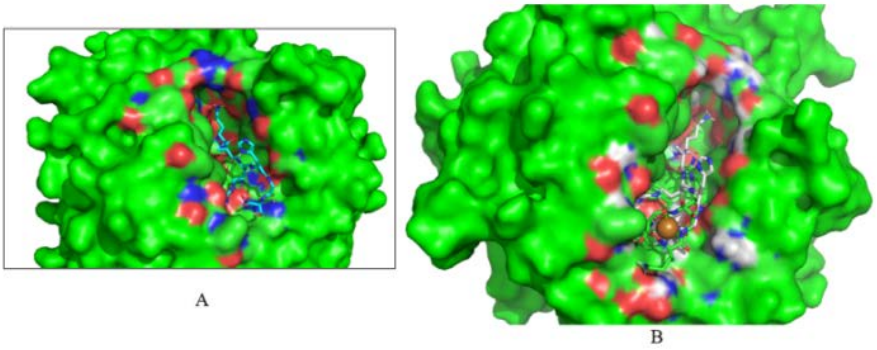

Figure 5. Metal-mediated "interaction saturation" of FLK11 in the catalytic groove of exo-β-(1,3)-glucanase. Surface representation of C. albicans exo-β-(1,3)-glucanase (green) with electrostatic potential mapped (red = anionic, blue = cationic). (A) Uncomplexed FLK11 bound within the catalytic groove, showing partial occupancy of the negatively charged channel and limited penetration toward the catalytic residues. (B) FLK11–Cu^{2+} complex bound in the same pocket, in which metal coordination rigidifies the peptide and positions a cationic side chain deeper into the anionic groove, resulting in enhanced electrostatic complementarity and increased hydrogen-bonding and salt-bridge contacts ("interaction saturation"). The Cu^{2+} ion is shown as an orange sphere; peptides are rendered as sticks

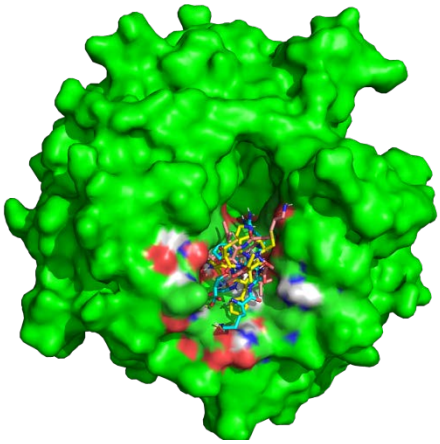

Figure 6. Convergent high-affinity binding modes of top-performing Cu^{2+}–peptide complexes in the catalytic groove of exo-β-(1,3)-glucanase. Surface representation of C. albicans exo-β-(1,3)-glucanase (green) with electrostatic potential mapped (red = anionic, blue = cationic). The two highest-ranking metallopeptide inhibitors—FLK12–Cu^{2+} (yellow sticks) and FLK6–Cu^{2+} (brown sticks)—are superposed within the catalytic groove, revealing convergent positioning within the anionic channel and extensive overlap of interaction hotspots. Metal coordination rigidifies the peptides and promotes deep penetration into the negatively charged pocket, enabling multi-point electrostatic anchoring and hydrogen-bond saturation consistent with the large affinity gains observed upon Cu^{2+} complexation. Cu^{2+} ions are shown as orange spheres

Table 4. summarizes key interactions for selected peptides against PBP1B, highlighting why uncomplexed peptides succeed and why Cu^{2+} complexation generally impairs binding

Ligand	Binding Affinity (kcal/mol)	Hydrogen Bonds	Electrostatic Interactions	Hydrophobic Pocket Occupation	Active-Site Proximity
FLK1	−6.9	3	1	Moderate	Yes
FLK5	−7.0	4	1	Strong	Yes
FLK11	−6.5	3	2	Moderate	Yes
FLK13	−6.8	4	2	Strong	Yes
FLK14	−6.9	3	1	Moderate	Yes
Moenomycin	−9.1	5	2	Strong	Yes
Acyl-cephalexin	−7.4	4	2	Moderate	Yes

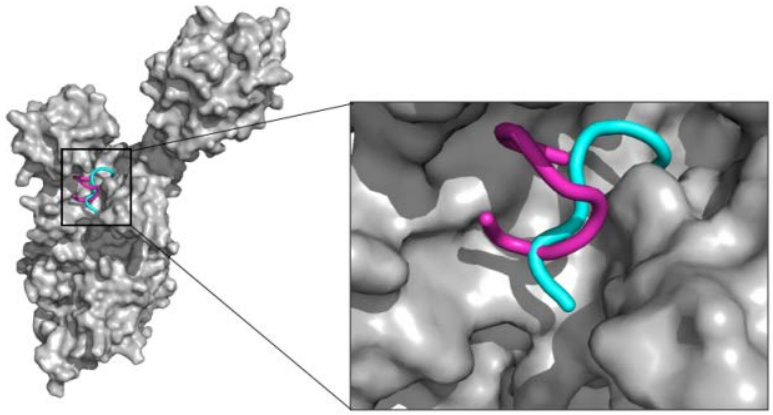

Figure 7. Binding modes of top-performing uncomplexed FLK peptides in the PBP1B transglycosylase groove. Representative docking poses of FLK5 (cyan) and FLK13 (magenta) within the hydrophobic transglycosylase channel of penicillin-binding protein 1B (PBP1B). Both peptides adopt extended conformations that enable deep penetration into the narrow binding groove and establish a balanced interaction network combining hydrogen bonding and hydrophobic pocket occupation. The superposed poses illustrate how uncomplexed FLK peptides can conformationally adapt to the constrained topology of the PBP1B active site, providing a structural rationale for their superior binding relative to the rigid Cu^{2+}–peptide complexes, which are sterically excluded from this pocket

3.6. Target Selectivity and Implications for Pathogen-Selective Therapy

The contrasting effects of Cu^{2+} complexation on PBP1B and glucanase highlight the potential for pathogen-selective modulation. FLK11 from pawpaw defensin exemplifies this dual behavior: as an uncomplexed peptide, it binds PBP1B with moderate affinity (−6.5 kcal/mol), whereas the Cu^{2+}–peptide complex exhibits strong glucanase binding (−14.81 kcal/mol) but severely reduced PBP1B affinity (−3.99 kcal/mol). This suggests that FLK11 retains structural plasticity, enabling adaptation to distinct enzymatic pockets, with target selectivity effectively "switched" by metal coordination.

Mechanistically, the quasi-spherical Cu^{2+}–peptide complex increases rigidity and steric bulk, which limits penetration into the narrow, hydrophobically dominated PBP1B groove. In contrast, the same metal complex enhances the peptide's interaction network with glucanase by enabling a more saturated network of hydrogen bonds and electrostatic contacts. Thus, steric and surface-charge distributions, rather than individual coordinating residues, govern target specificity under this model.

This selective behavior is of practical interest for antifungal therapy, as it could maximize pathogen inhibition while minimizing off-target effects on beneficial bacteria. Supporting this concept, recent studies report that Cu(II) complexes of human CCL-28 fragments display potent activity against C. albicans at pH 5.4 [23]. Furthermore, the pH-dependent coordination properties of Cu(II)-peptide complexes [22] may provide additional selectivity, exploiting the slightly acidic microenvironments characteristic of fungal infection sites. Taken together, these findings demonstrate that metal-mediated modulation of peptide structure can be leveraged to design highly selective, dual-target antimicrobial agents.

3.7. Identification of Lead Candidates for Experimental Validation

Based on the integrated analysis of docking binding affinities (Tables 2) and the detailed protein–ligand interaction fingerprints (Table 3 and Table 4), a refined panel of lead candidates was selected for downstream experimental validation. These candidates, summarized in Table 5, represent the optimal balance of binding energy, interaction stability, and target accessibility for each respective protein. Particular emphasis was placed on pawpaw defensin derivatives, which consistently yielded high-performing ligands across both uncomplexed and Cu^{2+}-complexed series.

Table 5. Top Lead Candidates Identified for Experimental Validation

Target Protein	Lead Peptides	Lead Cu^{2+} Complexes
Exo-β-(1,3)-glucanase	FLK4 (maize), FLK13 (tomato)	FLK11–Cu^{2+} (pawpaw), FLK12–Cu^{2+} (tomato)
PBP1B	FLK1 (avocado), FLK5 (pawpaw), FLK11 (pawpaw), FLK13 (tomato), FLK14 (tomato)	None

Exo-β-(1,3)-Glucanase

Among uncomplexed peptides, FLK4 (maize defensin) and FLK13 (tomato defensin) were selected as reference ligands. Although their intrinsic affinities (≈ −7.5 kcal/mol) are modest relative to the metallopeptides, both consistently engage the catalytic site with 3–4 hydrogen bonds and key electrostatic contacts. These peptides therefore provide essential controls for quantifying the specific contribution of Cu^{2+} complexation to inhibitory potency.

The primary antifungal candidates are the Cu^{2+}–peptide complexes FLK11–Cu^{2+} (pawpaw defensin) and FLK12–Cu^{2+} (tomato defensin). These complexes exhibited pronounced interaction saturation, forming 5–6 hydrogen bonds and 3–4 electrostatic contacts (Table 5), which directly correlated with sub −13 kcal/mol binding energies. FLK11–Cu^{2+}, with the strongest affinity (−14.81 kcal/mol) and most extensive interaction network, emerges as the top-priority candidate for enzymatic inhibition assays.

Notably, the comparison between FLK11–Cu^{2+} and FLK5–Cu^{2+} (the cysteine-containing analogue of the same core sequence) remains mechanistically informative, enabling experimental evaluation of how side-chain

composition modulates binding enhancement within the same backbone-centric metal coordination framework.

PBP1B

In accordance with the steric exclusion model established in Sections 3.3–3.5, no Cu^{2+} complexes were advanced for PBP1B validation. Instead, five uncomplexed peptides—FLK1 (avocado defensin), FLK5 (pawpaw defensin), FLK11 (pawpaw defensin), FLK13 (tomato defensin), and FLK14 (tomato defensin)—were selected as the most promising antibacterial leads. These peptides share three defining features:

(i) binding affinities comparable to acyl-cephalexin,

(ii) balanced interaction fingerprints combining hydrogen bonding with effective hydrophobic pocket occupation, and

(iii) consistent active-site accessibility (Table 6).

The inability of Cu^{2+}–peptide complexes to penetrate the narrow hydrophobic groove of PBP1B underscores the importance of molecular flexibility and steric compatibility for this target.

Dual-Target Scaffold Potential

The inclusion of FLK11 in both the glucanase (Cu^{2+}–complexed) and PBP1B (uncomplexed) lead panels is particularly noteworthy, Figure 8 shows the binding mode of FLK 11 with the two proteins (well fitted in the binding groves of both). This dual behavior positions FLK11 as a versatile scaffold for pathogen-selective inhibitor development, with metal coordination functioning as a switchable modality that redirects target specificity. Collectively, these findings identify pawpaw defensin Pdf1.1 as the most productive source of bioactive fragments in this study, yielding multiple active peptides (FLK5, FLK6, FLK11) and the top-performing metallopeptide (FLK11–Cu^{2+}).

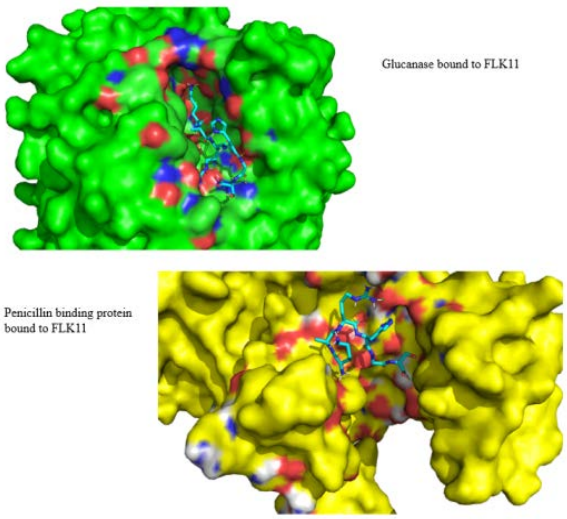

Figure 8. Overall binding pose comparison of uncomplexed FLK11 with both target enzymes. (Top) Glucanase-bound FLK11 (cyan sticks) within the catalytic pocket of exo-β-(1,3)-glucanase (green surface). (Bottom) PBP1B-bound FLK11 (cyan sticks) within the transglycosylase groove of PBP1B (yellow surface). The peptide is well-fitted in the binding grooves of both proteins, adopting distinct conformations optimized for each active-site architecture. This dual behavior positions FLK11 as a versatile scaffold for pathogen-selective inhibitor development, with metal coordination functioning as a switchable modality that redirects target specificity

3.8. Limitations and Future Directions

While molecular docking provides valuable first-order insights into relative binding trends and interaction fingerprints, several limitations inherent to the present computational framework should be acknowledged. First, docking scores represent approximate surrogates of binding free energy and cannot fully capture entropic contributions, solvent effects, or long-timescale conformational dynamics. Benchmarking studies on peptide–protein docking indicate that although pose sampling is often reasonable, scoring functions exhibit limited accuracy in predicting absolute binding affinities, reinforcing the need for experimental validation and complementary molecular dynamics simulations to assess binding stability over time.

Second, the docking protocol employed here treats the protein targets as rigid receptors. This approximation neglects potential induced-fit effects that may be particularly relevant for flexible peptide ligands and for enzymes such as PBP1B, whose active-site groove can undergo conformational adjustment upon ligand engagement. Future studies employing ensemble docking and explicit molecular dynamics sampling would provide a more realistic representation of receptor adaptability.

Third, the native membrane environment of PBP1B was not explicitly modeled. As PBP1B is a membrane-associated enzyme, the lipid bilayer may influence the accessibility and geometry of the transglycosylase groove, as well as the steric constraints governing ligand entry. Incorporation of membrane-embedded protein models in future simulations will therefore be important for refining predictions of antibacterial activity.

Fourth, the Cu^{2+}–peptide complexes were constructed using a backbone-centric coordination model designed to preserve surface exposure of side chains and minimize bias toward predefined chelation motifs. While this abstraction enables systematic comparison of docking outcomes across diverse peptides, it does not capture the full electronic complexity of Cu^{2+} coordination chemistry. Consequently, the modeled complexes should be interpreted as functional docking surrogates rather than definitive representations of solution-phase coordination geometries. Experimental validation using spectroscopic techniques (e.g., UV–Vis, EPR, circular dichroism) will be essential to establish the dominant coordination modes of synthesized FLK–Cu^{2+} complexes and to relate coordination behavior to biological activity.

Future work would prioritize:

(i) chemical synthesis of lead peptides and their Cu^{2+} complexes, particularly pawpaw-derived FLK5, FLK6, and FLK11;

(ii) spectroscopic characterization of Cu^{2+} coordination environments;

(iii) antifungal and antibacterial activity assays against representative fungal (Candida albicans) and bacterial (Escherichia coli) strains;

(iv) cytotoxicity profiling in mammalian cell models to assess therapeutic windows;

(v) evaluation of ROS generation as a potential secondary antifungal mechanism for Cu^{2+} complexes; and

(vi) molecular dynamics simulations to interrogate binding stability, steric accessibility, and target-specific conformational adaptation.

Collectively, these studies will be essential to translate the present *in-silico* findings into experimentally validated lead compounds for antifungal and antibacterial development.

4. Conclusion

This study demonstrates that short peptides derived from cationic clusters of defensins from Nigerian edible plants retain potent enzyme-binding capacity, validating a rational design strategy that transforms complex natural products into synthetically accessible antimicrobial leads. The FLK peptide library exhibited strong sequence-dependent binding to both fungal and bacterial targets, with several uncomplexed peptides achieving affinities comparable to established inhibitors. Cu^{2+} complexation produced diametrically opposed effects—dramatic enhancement for exo-β-(1,3)-glucanase versus catastrophic disruption for PBP1B—highlighting the importance of target architecture in determining whether metal complexation is beneficial or detrimental to binding.

The pawpaw defensin Pdf1.1 emerged as an exceptionally rich source of bioactive peptide scaffolds, yielding four derivatives, including the top-performing metal complex FLK11–Cu^{2+}, which achieved ultra-high affinity (−14.81 kcal/mol) through interaction saturation (six hydrogen bonds and four electrostatic contacts). The overlapping fragments derived from this defensin (FLK5 with a terminal cysteine versus FLK11 without cysteine) provide valuable insight into structure–activity relationships. Under the backbone-centric Cu^{2+} coordination model used here, the superior performance of FLK11–Cu^{2+} suggests that the absence of cysteine promotes a more favorable surface charge distribution and steric presentation of side chains toward the glucanase catalytic pocket, rather than improved metal chelation per se.

For exo-β-(1,3)-glucanase, FLK11–Cu^{2+} and FLK12–Cu^{2+} represent the most promising antifungal leads, exhibiting pronounced interaction saturation and deep engagement of the catalytic site. In contrast, inhibition of PBP1B favored uncomplexed peptides from avocado (FLK1), pawpaw (FLK5, FLK11), and tomato (FLK13, FLK14), with Cu^{2+} complexation consistently impairing binding due to increased rigidity and steric incompatibility within the narrow hydrophobic transglycosylase groove.

Collectively, these findings establish a structure–activity framework for the rational design of pathogen-selective metallopeptide inhibitors, demonstrating that metal coordination can function as a tunable switch for target selectivity rather than a universally beneficial modification. The successful translation of defensin motifs from Nigerian edible plants—particularly pawpaw (Pdf1.1)—into short, amphiphilic peptides with high enzyme-binding potency represents an important step toward developing locally sourced, chemically accessible antimicrobial leads for experimental validation and therapeutic development.

References

[1] Amerikova, M., Pencheva El-Tibi, I., Maslarska, V., Bozhanov, S., & Tachkov, K. (2025). Antimicrobial activity, mechanism of action, and methods for stabilisation of defensins as new therapeutic agents. MTMT.

[2] Fu, J., Zong, X., Jin, M., Min, J., Wang, F., & Wang, Y. (2023). Mechanisms and regulation of defensins in host defense. Signal Transduction and Targeted Therapy, 8(1).

[3] Liu, Y., *et al*. (2025). Structure, function, and therapeutic potential of defensins from marine animals. Fish and Shellfish Immunology, 163, 110365.

[4] Nature Communications. (2023). Plant immunity suppression by an exo-β-1,3-glucanase and an elongation factor 1α of the rice blast fungus. Nature Communications, 14, 5491.

[5] Yeaman, M. R., & Yount, N. Y. (2003). Mechanisms of antimicrobial peptide action and resistance. Pharmacological Reviews, 55(1), 27–55.

[6] Brogden, K. A. (2005). Antimicrobial peptides: pore formers or metabolic inhibitors in bacteria? Nature Reviews Microbiology, 3(3), 238–250.

[7] Matsuzaki, K. (2009). Control of cell selectivity of antimicrobial peptides. Biochimica et Biophysica Acta (BBA)-Biomembranes, 1788(8), 1687–1692.

[8] Porto, W. F., & Franco, O. L. (2013). Theoretical structural insights into the snakin family of antimicrobial peptides. Biopolymers, 100(5), 485–495.

[9] Seo, H. H., Park, S., Park, S., Oh, B. J., Back, K., Han, O., & Kim, J. I. (2014). Overexpression of a defensin enhances resistance to a fruit-specific anthracnose fungus in pepper. PLoS ONE, 9(5), e97982.

[10] Jaquelina, G. R., *et al*. (2013). PaDef, a plant defensin from avocado (Persea americana) with antimicrobial activity. Peptides, 44, 18–24.

[11] Kwon, R. S., *et al*. (2024). Tomato tdAmp1 defensin: Structural characterization and antimicrobial mechanism. Journal of Agricultural and Food Chemistry, 72(3), 1452–1463.

[12] Rivera-D, M., *et al*. (2012). Pdf1.1 defensin from Carica papaya: Characterization and antifungal activity. Plant Physiology and Biochemistry, 56, 41–48.

[13] Baosheng, L., *et al*. (2011). ZMDEF1, a maize defensin with antifungal activity. Journal of Plant Biology, 54(3), 181–188.

[14] Hancock, R. E., & Sahl, H. G. (2006). Antimicrobial and host-defense peptides as new anti-infective therapeutic strategies. Nature Biotechnology, 24(12), 1551–1557.

[15] Fjell, C. D., Hiss, J. A., Hancock, R. E., & Schneider, G. (2012). Designing antimicrobial peptides: form follows function. Nature Reviews Drug Discovery, 11(1), 37–51.

[16] Nguyen, L. T., Haney, E. F., & Vogel, H. J. (2011). The expanding scope of antimicrobial peptide structures and their modes of action. Trends in Biotechnology, 29(9), 464–472.

[17] Tossi, A., Sandri, L., & Giangaspero, A. (2000). Amphipathic, α-helical antimicrobial peptides. Biopolymers, 55(1), 4–30.

[18] Merrifield, R. B. (1963). Solid phase peptide synthesis. I. The synthesis of a tetrapeptide. Journal of the American Chemical Society, 85(14), 2149–2154.

[19] Boman, H. G. (2003). Antibacterial peptides: basic facts and emerging concepts. Journal of Internal Medicine, 254(3), 197–215.

[20] Falcigno, L., Braccia, S., Bellavita, R., D'Auria, G., Falanga, A., & Galdiero, S. (2024). Metal-antimicrobial peptides combo: promising weapons to combat bacteria invaders. Frontiers in Drug Discovery, 4, 1440378.

[21] Hureau, C., Da Costa Ferreira, A. M., & Facchin, G. (Eds.). (2024). Editorial Board Members' Collection Series in "Bioinorganic Chemistry of Copper". MDPI Books.

[22] Kozlowski, H., Bal, W., Dyba, M., & Kowalik-Jankowska, T. (1999). Specific structure–stability relations in metallopeptides. Coordination Chemistry Reviews, 184(1), 319–346.

[23] Szarszoń, K., *et al*. (2024). Bioinorganic Chemistry Meets Microbiology: Copper(II) and Zinc(II) Complexes Doing the Cha-Cha with the C-t-CCL-28 Peptide, Dancing till the End of Microbes. Inorganic Chemistry, 63(41), 19105–19116.

[24] Candida Genome Database. (1999). XOG1 (C. albicans) exo-β-(1,3)-glucanase structure and function.

[25] Cutfield, S. M., Davies, G. J., Murshudov, G., Anderson, B. F., Moody, P. C., Sullivan, P. A., & Cutfield, J. F. (1999). The structure of the exo-β-(1,3)-glucanase from Candida albicans in native and bound forms: relationship between a pocket and groove in family 5 glycosyl hydrolases. Journal of Molecular Biology, 294, 771–783.

[26] Sung, M. T., Lai, Y. T., Huang, C. Y., Chou, L. Y., Shih, H. W., Cheng, W. C., & Ma, C. (2009). Crystal structure of the membrane-bound bifunctional transglycosylase PBP1b from Escherichia coli. Proceedings of the National Academy of Sciences, 106(22), 8824–8829.

[27] Dik, D. A., *et al*. (2019). Slt, MltD, and MltG of Pseudomonas aeruginosa as Targets of Bulgecin A in Potentiation of β-Lactam Antibiotics. ACS Chemical Biology, 14(2), 296–303.

[28] PMC. (2008). Domain requirement of moenomycin binding to bifunctional transglycosylases and development of high-throughput discovery of antibiotics. Proceedings of the National Academy of Sciences, 105(2), 431–436.

[29] Singh, B. P., Paul, S., Ferreira-Santos, P., Bhushan, B., Hati, S., Goel, G., & Udenigwe, C. (2025). In silico and molecular docking approaches in food-derived bioactive peptide discovery: Trends, challenges, and prospects. Food Research International.

[30] ScienceDirect. (2025). Innovative strategies for modeling peptide–protein interactions and rational peptide drug design. Current Opinion in Structural Biology.

[31] Zhao, H., Jiang, D., Shen, C., Zhang, J., Zhang, X., Wang, X., Nie, D., Hou, T., & Kang, Y. (2024). Comprehensive Evaluation of 10 Docking Programs on a Diverse Set of Protein–Cyclic Peptide Complexes. Journal of Chemical Information and Modeling.

[32] Yuan, S., Chan, H. S., & Hu, Z. (2017). Using PyMOL as a platform for computational drug design. Wiley Interdisciplinary Reviews: Computational Molecular Science, 7(2), e1298.

[33] Morris, G. M., Huey, R., Lindstrom, W., Sanner, M. F., Belew, R. K., Goodsell, D. S., & Olson, A. J. (2009). AutoDock4 and AutoDockTools4: Automated docking with selective receptor flexibility. Journal of Computational Chemistry, 30(16), 2785–2791.

[34] Trott, O., & Olson, A. J. (2010). AutoDock Vina: improving the speed and accuracy of docking with a new scoring function, efficient optimization, and multithreading. Journal of Computational Chemistry, 31(2), 455–461.

[35] Sigel, H., & Martin, R. B. (1982). Coordinating properties of the amide bond. Stability and structure of metal ion complexes of peptides and related ligands. Chemical Reviews, 82(4), 385–426.

[36] Santos-Martins, D., Forli, S., Ramos, M. J., & Olson, A. J. (2014). AutoDock4(Zn): an improved AutoDock force field for small-molecule docking to zinc metalloproteins. Journal of Chemical Information and Modeling, 54(8), 2371–2379.

[37] Seeliger, D., & de Groot, B. L. (2010). Ligand docking and binding site analysis with PyMOL and Autodock/Vina. Journal of Computer-Aided Molecular Design, 24(5), 417–422.

[38] Craik, D. J., Fairlie, D. P., Liras, S., & Price, D. (2013). The future of peptide-based drugs. Chemical Biology & Drug Design, 81(1), 136–147.

[39] Engineering. (2024). Incorporating Single-Copper Sites and Host Defense Peptides into a Nanoreactor for Antibacterial Therapy by Bioinspired Design. Engineering.